applied optics

Wavelength optimization using available laser diodes in spectral near-infrared optical tomography

Liang-Yu Chen,[1,2] Min-Cheng Pan,[3] Chung-Chen Yan,[1] and Min-Chun Pan[1,2,*]

[1]Department of Mechanical Engineering, National Central University, Taoyuan City 320, Taiwan
[2]Graduate Institute of Biomedical Engineering, National Central University, Taoyuan City 320, Taiwan
[3]Department of Electronic Engineering, Tung-Nan University, New Taipei City 222, Taiwan
*Corresponding author: pan_minc@cc.ncu.edu.tw

Received 1 March 2016; revised 23 April 2016; accepted 25 April 2016; posted 25 April 2016 (Doc. ID 260272); published 18 July 2016

For employing optimized wavelengths, a near-infrared (NIR) tomographic imaging system with multiwavelengths in a continuous wave (CW) enables us to provide accurate information of chromophores. In this paper, we discuss wavelength optimization with a selection from commercial laser diodes. Through theoretical analysis, the residual norm (R) and the condition number (κ) represent the uniqueness of a matrix problem and the smooth singular-value distribution of each chromophore, respectively. The optimum wavelengths take place for large R and small κ. We considered a total of 38 wavelengths of laser diodes in the range of 633–980 nm commercially available to discover optimum sets for a broad range of chromophore combinations. In the 38 wavelengths, there exists 501,942 (C_5^{38}), 2,760,681 (C_6^{38}), and 12,620,256 (C_7^{38}) combinations of five, six, and seven wavelength sets, respectively, for accurately estimating chromophores (HbO_2, HbR, H_2O, and lipids), water, lipids, and the scattering prefactor A. With the numerical calculation, the top 10 wavelength sets were selected based on the principle of large R and small κ. In the study, the chromophore concentration for young and elderly women are investigated; finally, choosing the laser diodes with a wavelength of 650, 690, 705, 730, 870/880, 915, and 937 nm is recommended either for young or elderly women to construct a spectral NIR tomographic imaging system in the CW domain. Simulated data were used to validate the claims.

OCIS codes: (170.0170) Medical optics and biotechnology; (170.2655) Functional monitoring and imaging; (290.1990) Diffusion.

http://dx.doi.org/10.1364/AO.55.005729

1. INTRODUCTION

As optimized wavelengths are employed, a near-infrared (NIR) tomographic imaging system with multiwavelengths in a continuous wave (CW) has the potential to provide accurate information of chromophores (oxyhemoglobin [HbO_2], deoxyhemoglobin [HbR], water [H_2O], and lipid) through diminishing cross talk between these parameters.

Prior to the method of determining optimum wavelength sets to be developed, the use of two wavelengths to investigate the uncertainties of the concentration changes in hemoglobin has been studied. Pairing a shorter wavelength with 830 nm can provide better sensitivity because of the larger difference in absorption coefficients of hemoglobin between two wavelengths. Because the uncertainties of the concentration changes in hemoglobin depend on the wavelength pair, the use of two-wavelength analysis was demonstrated with one wavelength fixed at 830 nm; a simultaneous measurement system using seven laser diodes from red to near-infrared light (664–848 nm) also was developed for spectroscopic measurement [1]. To detect changes in the concentration of oxygenated hemoglobin and deoxygenated hemoglobin in tissue, a simultaneous recording system of near-infrared spectroscopy was conducted at five wavelengths (678, 692, 750, 782, and 830 nm) to determine the best wavelength for pairing with 830 nm [2]. A scanning system was utilized on the acquisition of time-resolved transmittance curves at 683, 785, 912, and 975 nm, thereby discriminating breast structures and lesions based on different absorption and scattering properties as well as reflecting different contributions of oxyhemoglobin, deoxyhemoglobin, water, lipids, and distinct structures [3]. As one wavelength is chosen below 720 nm while the other is greater than 730 nm, cross talk is low and separability is high to result in accurate concentration changes, thereby determining the concentration changes in HbO_2 and HbR with a two-wavelength near-infrared spectroscopy system between 610 and 920 nm [4]. In late gated intensity images, the mammary gland or its residual in elderly women, can usually be detected as a strongly attenuating structure at 975 nm; blood vessels are clearly detected as highly

absorbing structures at 683 and 785 nm, where blood absorption is higher. Further, lipomas strongly attenuate light at 913 nm, i.e., close to the absorption peak of lipids at 930 nm. A time-resolved optical mammography operating at 683, 785, 913, and 975 nm was used in a clinical trial in detecting and characterizing breast lesions [5].

To date, two research groups [6–8] have conducted and published relevant studies about the optimum wavelength sets with a completely theoretical analysis. One is that the wavelengths were chosen in the range of 650–930 nm, spaced in 6 nm intervals, and the others discussed six discrete wavelengths selected from the entire spectral range of 650–930 nm with a separation of 4 nm. Mainly, the light was provided by mode-locked lasers, for instance, dye or Ti:Sapphire lasers, which were sequentially tuned to cover the range from 600 up to 1000 nm. With an extension to the method [6], an additional criterion of the wavelength optimization approach was presented by considering the uncertainties in the absorption spectra of the chromophores [9]. Simulation tasks were performed to image breast cancer by combining spatial and spectral priors, where magnetic resonance images of water and lipid content were used as a statistical spatial prior, and wavelengths were chosen to keep the condition number of the extinction matrix small [10].

Though these analyses are useful, their laser systems were, however, constructed by tuning with a fixed interval of 4 or 6 mm. This implies that an expensive laser system was operated. Instead, lots of commercialized laser diodes can be obtained in the market and are economical, low-cost maintenance, and miniaturized. Therefore, in this paper we investigate wavelength optimization through using these available laser diodes.

In the following, Section 2 describes the theoretical method of wavelength optimization. Subsequently, we present five, six, and seven optimized wavelengths for the estimation of four optical parameters—HbO_2, HbR, H_2O, and lipid—which are identified through theoretical analysis of 38 commercially available wavelengths in total. Finally, concluding remarks are given.

2. METHOD

In this section, we show how this nonuniqueness problem associated with CW imaging can be overcome, provided the spectral approach is used with the optimal measurement wavelengths. The diffusion equation of continuous wave light can be written as

$$\nabla \cdot D(\mathbf{r})\nabla\Phi(\mathbf{r}) - \mu_a(\mathbf{r})\Phi(\mathbf{r}) = -S(\mathbf{r}), \quad (1)$$

where $\Phi(\mathbf{r})$ is the photon density at position $\boldsymbol{r}$, $S(\mathbf{r})$ is the isotropic source term, and μ_a and D denote the optical absorption and diffusion coefficients, respectively. Further, D is equal to $1/3(\mu_a + \mu')_s$ where μ_s' is the reduced scattering coefficient. Given a set of boundary data at a given wavelength, the aim of the inverse problem is to recover the distribution of optical parameters in tissue. The finite element forward solver of Eq. (1) can be obtained with the substitution of Φ, D, and μ_a expanded as the sum of coefficients multiplied by a set Lagrangian basis function as well as the discretization with integration over the problem domain accompanied by the boundary-condition-applied surface. Subsequently, Φ can be achieved from the equation in a matrix from; furthermore, the first derivative of Φ relating to optical parameters (D and μ_a) can be derived. Readers can see more details in [11].

To form an iterative equation for estimating the increment from a uniform distribution of the optical property, by using the first-order Taylor series to expand $\mathbf{\Phi}$, one can obtain

$$(\mathbf{\Phi}^M) \approx (\mathbf{\Phi}^C) + \left[\frac{\partial \mathbf{\Phi}^C}{\partial \boldsymbol{\mu}_a}\right](\Delta\boldsymbol{\mu}_a) + \left[\frac{\partial \mathbf{\Phi}^C}{\partial D}\right](\Delta D), \quad (2)$$

where $\mathbf{\Phi}^M$ is the measured data and $\mathbf{\Phi}^C$ is the calculated data from the forward model. From Eq. (2), the inverse problem can be formulated as

$$\begin{bmatrix} \frac{\partial \mathbf{\Phi}^C}{\partial \boldsymbol{\mu}_a} & \frac{\partial \mathbf{\Phi}^C}{\partial D} \end{bmatrix} \begin{pmatrix} \Delta\boldsymbol{\mu}_a \\ \Delta D \end{pmatrix} = (\mathbf{\Phi}^M - \mathbf{\Phi}^C), \quad (3)$$

or simply denoted as $\mathbf{J}\Delta\boldsymbol{\chi} = \Delta\mathbf{\Phi}$, where $\mathbf{J} = \left[\partial\mathbf{\Phi}^C/\partial\boldsymbol{\mu}_a \quad \partial\mathbf{\Phi}^C/\partial D\right]$ is the Jacobian matrix, i.e., the rate of change of model data with respect to optical parameters, and $\Delta\boldsymbol{\chi}$ means $(\Delta\boldsymbol{\mu}_a; \Delta\mathbf{D})$, the increment of optical parameters. The goal of Eq. (3) is to reach the measured data $\mathbf{\Phi}^M$ from the calculated data $\mathbf{\Phi}^C$ estimated from the forward model, i.e., minimizing the difference between the measured data and the calculated data while estimating optical parameters, μ_a and D, with the increment variation. However, such an inverse problem is nonlinear and ill-posed; to cope with this, Tikhonov regularization is usually applied. Therefore, the inverse problem is formulated as an optimization of the damped least-squares problem:

$$\min_{\Delta\boldsymbol{\chi}}\{Q_{Tk}(\Delta\boldsymbol{\chi})\} = \min_{\Delta\boldsymbol{\chi}}\{\|\mathbf{J}\Delta\boldsymbol{\chi} - \Delta\mathbf{\Phi}\|_2^2 + \lambda^2\|\mathbf{L}\Delta\boldsymbol{\chi}\|_2^2\}, \quad (4)$$

where $\mathbf{L}$ is the dimensionless regularization matrix and λ is the regularization parameter. Specifically, Eq. (4) is called the zero-order Tikhonov regularization, provided that the identity matrix is adopted as the regularization matrix, i.e., $\mathbf{L} = \mathbf{I}$. Subsequently, Eq. (5) can be obtained as

$$(\mathbf{J}^T\mathbf{J} + \lambda^2\mathbf{I})\Delta\boldsymbol{\chi} = \mathbf{J}^T\Delta\mathbf{\Phi}. \quad (5)$$

Generally, Eq. (5) is the basic calculation widely used for the inverse problem to estimate the optical parameters (μ_a and D) of a high-scattering matter injected with a light.

As known from Beer's law, the absorption coefficient at a given wavelength can be formulated by a linear combination of the extinction coefficients (ε) [12] and their corresponding chromophore concentrations (C), i.e.,

$$\mu_a(\lambda_n) = \sum_{i=1}^{L} \varepsilon_i(\lambda_n)C_i, \quad (6)$$

where i denotes the ith chromophore, L is the number of chromophores to be considered, and λ_n is the nth wavelength. It is noted that N wavelengths of laser diodes are used. The reduced scattering parameter can be empirically given by

$$\mu_s'(\lambda) = A\lambda^{-s_p}, \quad (7)$$

where A is the scattering amplitude and s_p is the scattering power.

Instead of using conventional methods to estimate the optical properties at each wavelength and then spectrally recover the chromophore concentrations and scattering parameters through Eqs. (6) and (7), we can incorporate these constraints into the reconstruction scheme to directly determine chromophore concentrations, scattering amplitude, and scattering power. Assume that we know $J_{\mu_a,\lambda} = \partial\Phi_\lambda/\partial\mu_a$ and $J_{D,\lambda} = \partial\Phi_\lambda/\partial D$, as shown in Eq. (3), in the spectrally constrained reconstruction the measurements at all wavelengths are coupled together, and the relations in Eqs. (6) and (7) are combined to create a new set of relations, which for each wavelength is represented by [6]

$$J_{c,\lambda}\Delta c + J_{A,\lambda}\Delta a + J_{s_p,\lambda}\Delta b = \Delta\Phi_\lambda, \tag{8}$$

where

$$J_{c,\lambda} = \begin{bmatrix} \varepsilon_1(\lambda) & \cdots & \varepsilon_L(\lambda) \end{bmatrix} \otimes J_{\mu_a,\lambda},$$
$$J_{A,\lambda} = (-3D^2)(\lambda^{-s_p})J_{D,\lambda},$$
$$J_{s_p,\lambda} = (3D^2)(\mu_s')(\ln\lambda)J_{D,\lambda},$$

and $\otimes$ refers to the Kronecker tensor product. Then, the overall system of equations solved during reconstruction can be assembled as

$$\begin{bmatrix} J_{c_1,\lambda_1} & \cdots & J_{c_L,\lambda_1} & J_{A,\lambda_1} & J_{s_p,\lambda_1} \\ & \ddots & & \vdots & \vdots \\ J_{c_1,\lambda_n} & \cdots & J_{c_L,\lambda_n} & J_{A,\lambda_n} & J_{s_p,\lambda_n} \end{bmatrix} \begin{pmatrix} \Delta c_1 \\ \vdots \\ \Delta c_L \\ \Delta A \\ \Delta s_p \end{pmatrix} = \begin{pmatrix} \Delta\Phi_{\lambda_1} \\ \vdots \\ \Delta\Phi_{\lambda_n} \end{pmatrix}, \tag{9}$$

where λ_1, …, and λ_n represent the light wavelengths we choose for measurement and reconstruction.

Through theoretical analysis [6], here we use the residual norm (R) and the condition number (κ) to represent the uniqueness of this matrix problem [Eq. (6)] and the smooth singular-value distribution of each chromophore, respectively. Both parameters can be defined as follows.

1. Uniqueness:

$$R = \|\mathbf{1} - \mathbf{E}(\mathbf{E}^{\mathbf{T}}\mathbf{E})^{-1}\mathbf{E}^{\mathbf{T}}\mathbf{1}\|, \tag{10}$$

where $\mathbf{E}$ is the extinction coefficient matrix normalized by the wavelength expressed as

$$\begin{bmatrix} \frac{\varepsilon_1(\lambda_1)}{\lambda_1^{s_p}} & \cdots & \frac{\varepsilon_L(\lambda_1)}{\lambda_1^{s_p}} \\ \cdots & \cdots & \cdots \\ \frac{\varepsilon_1(\lambda_N)}{\lambda_N^{s_p}} & \cdots & \frac{\varepsilon_L(\lambda_N)}{\lambda_N^{s_p}} \end{bmatrix}. \tag{11}$$

This indicates R is the norm of wavelength-dependent matrixes.

2. Condition number:

$$\kappa = \|\varepsilon(\lambda)\|\|\varepsilon^{-1}(\lambda)\|. \tag{12}$$

This indicates κ is the norm of the matrix of chromophore extinction coefficients.

As shown at the top-left corner in Fig. 1, it is known that the optimum wavelengths take place for large R and small κ. Further, R and κ can be interpreted as the distinguishability parameters representing the uniqueness and stability of solution, respectively. Maximizing the residual norm (R) for a unique solution and minimizing the condition number (κ) for each chromophore with similar contributions to absorption were used as criteria.

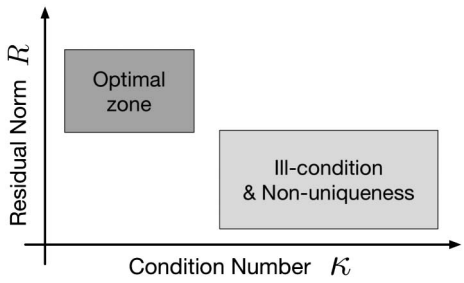

Fig. 1. Schematic of the optimum and worst zones of residual norm and condition number for uniqueness and smooth distribution of chromophores.

It is better to fix one of the scattering parameters; this assumption makes it possible to easily compute the matrix in Eq. (11) numerically with the scattering power $s_p = 1.3$ in our calculation. The absorption spectra are essential for reconstruction, provided absorption and scattering should be distinguishable in CW diffuse optical imaging (DOI).

For DOI of breast cancer, the dominant absorbing chromophores in the near infrared are oxyhemoglobin (HbO_2), deoxyhemoglobin (HbR), water (H_2O), and lipid, with the spectral variation for the absorption coefficient given by

$$\mu_a(\lambda_n) = \varepsilon_{\mathrm{HbO_2}}(\lambda_n)C_{\mathrm{HbO_2}} + \varepsilon_{\mathrm{HbR}}(\lambda_n)C_{\mathrm{HbR}} + \varepsilon_{\mathrm{H_2O}}(\lambda_n)C_{\mathrm{H_2O}} + \varepsilon_{\mathrm{lipid}}(\lambda_n)C_{\mathrm{lipid}}. \tag{13}$$

Here four chromophores are to estimate, and the scattering amplitude is allowed to vary, so that five wavelengths at least are required. In a typical DOI reconstruction scheme, three steps are performed to achieve the final HbO_2, HbR, H_2O, and lipid images. First, the measurements are taken simultaneously at five or more different wavelengths, second the images of the absorption coefficients at the different wavelengths are reconstructed separately, and, finally, the concentration of HbO_2, HbR, H_2O, and lipids are computed from the spectral variation in the absorption images.

3. RESULTS AND ANALYSIS

As described in the introduction, tunable laser systems were used in previous studies of wavelength optimization [6–9]; however, to the best of our knowledge, there is no analysis and discussion regarding those wavelengths of commercially available laser diodes. We considered a total of 38 wavelengths in the range of 633–980 nm available in the market (Table 1) to discover optimum wavelength sets for a broad range of chromophore combinations. Those laser diodes can be purchased from the following companies: Coherent Inc., Newport Corp., Omicron-Laserage, Ondax Inc., Power Technology Inc., Thorlab Inc., and Vortran Laser Technology Inc.

Table 1. Thirty-eight Wavelengths of Laser Diodes Ranging between 633 and 980 nm Available on the Market

Ranges (nm)	Wavelengths (nm)
633–650	633, 635, 636, 637, 638, 639, 640, 642, 643, 647, 650
651–699	655, 658, 660, 670, 685, 690
700–799	705, 730, 760, 773, 780, 785, 790
800–899	808, 816, 830, 850, 852, 860, 870, 880
900–980	905, 915, 937, 940,976, 980

Reported in [13], higher water and total hemoglobin content and lower lipid content were found in a young women's breast, while the oxygenation is comparable with that measured in older subjects. These findings are in agreement with the evolution of the female breast because lipids tend to increase with age at the expense of progressive reduction of the mammary gland. For comparison, in Table 2 we list our and another five groups' [HbO_2], [HbR], [H_2O], and [Lipid] used in the computation. Table 2 also shows that the chromophore characteristics of breasts in younger and older women were considered and investigated in this study. Moreover, it has been proven there that the optimal chromophore image reconstruction obtained is consistent with the theoretical expectations, of which the optimal wavelength sets are chosen according to the same criteria of large R and small κ from the plot by the computation of Eqs. (10) and (12).

The scatterplot of the residual and the condition number was calculated for four chromophores, hemoglobin and deoxyhemoglobin, water, and lipids. Selecting from a total of 38 wavelengths of laser diodes, there exists 501,942 (C_5^{38}), 2,760,681 (C_6^{38}), and 12,620,256 (C_7^{38}) sets of five, six, and seven wavelength combinations, respectively, for accurately estimating chromophores (HbO_2 and HbR), water, lipids, plus the scattering prefactor A. As shown in Figs. 3, 5, and 7, each point in the scatterplot represents a specific set of five, six, or seven wavelength combinations in the range of 633–980 nm; furthermore, their local upper-left parts are zoomed in, as shown in Figs. 4, 6, and 8, of which the highlighted regions satisfy the criteria of large residual and small condition numbers. When calculating κ and R for each set of wavelength combination, it is observed that κ distributes widely from 10 to 10^4, whereas R ranges between 0 and 1. As mentioned, the criteria for the selection of the optimum-wavelength sets here are satisfied with

$$\kappa_{ni} < 2\kappa_{\min} \quad \text{and then} \quad R_{n1} > R_{n2}, \qquad n1 < n2, \tag{14}$$

where $\kappa_{\min}$ is the minimum value of κ. Equation (14) expresses the κ value of the selected point ni, which is smaller than a user-defined threshold $2\kappa_{\min}$, and R_{n1} has a largest value of R.

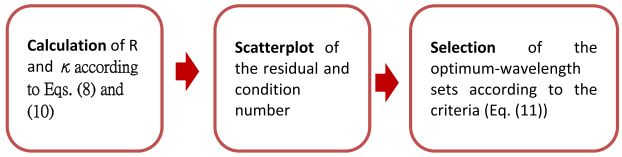

Fig. 2. Flow chart of selecting the optimal wavelength sets.

From the above description, a flow chart in Fig. 2 shows the steps to search the optimal wavelength sets for a spectral NIR tomographic imaging system in the CW domain to estimate chromophores (HbO_2 and HbR), water, and lipids.

In the following, the conditions of young and elderly women are investigated, respectively, in Sections 3.A and 3.B. As known, younger women usually have higher [H_2O] and lower [Lipid] than older women. Thus, in Section 3.A, [HbO_2], [HbR], [H_2O], and [Lipid] of young women are considered to be 20 μM, 10 μM, 50%, and 25%, whereas those of elderly women equal to 30 μM, 10 μM, 15%, and 85% are discussed in Section 3.B.

A. Under the Condition of Young Women

1. Five Wavelength Sets

We first consider optimum sets for the case of four absorption chromophores (HbO_2, HbR, H_2O, lipids) and five measurement wavelengths. Figure 3 shows all combinations of five wavelengths from all 38 wavelengths; however, only the optimal region in the upper-left part indicated by a red box will be selected.

For further investigation, Fig. 4 shows the points in the red box of Fig. 3 in which "∗" (green) is shown there to represent the position (κ, R) with the smallest κ and the biggest R; a threshold value line is plotted as well. The same indications are also displayed in the following cases. With the help of Fig. 4, top 10 different combination sets of five wavelengths (Table 3) can be selected from extreme points with large R and small κ, based on high R rather than only low κ.

As shown in Table 3, the top 10 optimal wavelength sets comprise 10 wavelengths of laser diodes: 650, 705, 730, 850, 852, 860, 870, 880, 915, and 937 nm. The wavelengths of 650, 705, 880, 915, and 937 nm are the first choices for the optimal wavelength set; further, it is noted that 870 or 880 nm is the only difference for the first or second choice.

2. Six Wavelength Sets

Steps are applied to the combination of six wavelengths to search the optimal wavelength sets according to the procedure of Fig. 2. Here, Fig. 5 illustrates the scatterplot of the residual and condition number of six wavelengths, and its zoomed-in plot for the optimal region is characterized in Fig. 6, where

Table 2. Concentrations of HbO_2, HbR, H_2O, and Lipids Used in this Study and the Other Groups

	Young Women	Elderly Women	[6]	[7]	[9]	[10]	[14]	[14]
[HbO_2]	20 μM	30 μM	20 μM	10 μM	10 μM	25 μM	29 μM	53 μM
[HbR]	10 μM	10 μM	10 μM	10 μM	5 μM	10 μM	8 μM	18 μM
[H_2O]	50%	15%	27%	18%	50%	40%	13%	46%
[Lipid]	25%	85%	25%		25%	30%	86%	29%

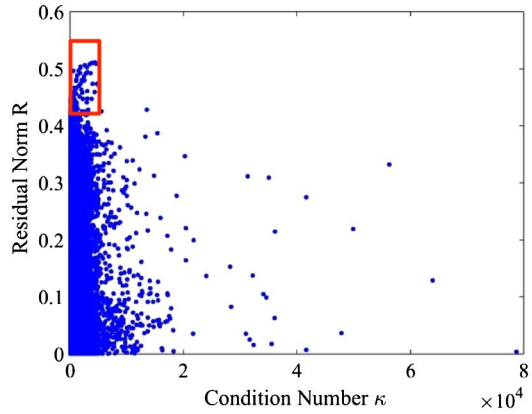

Fig. 3. Scatterplot of the residual and condition number; each point represents a different combination set of laser diodes with five wavelengths.

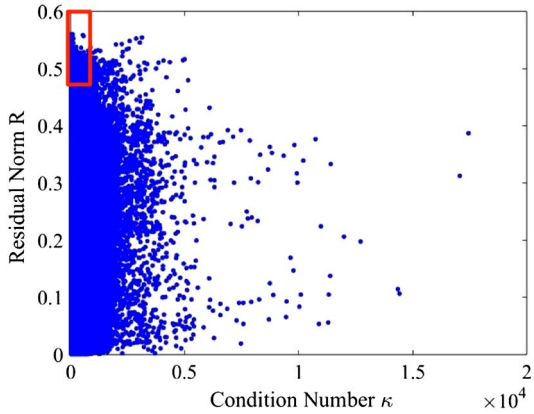

Fig. 5. Scatterplot of the residual and condition number; each point represents a different combination set of laser diodes wth six wavelengths.

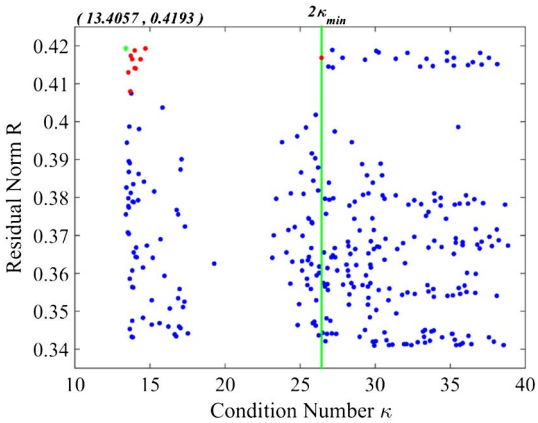

Fig. 4. Zoom-in illustration of Fig. 3.

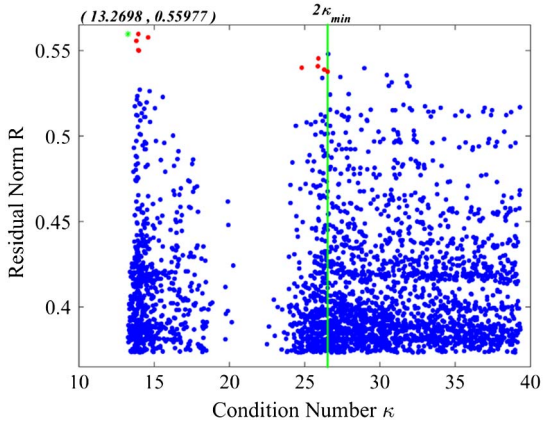

Fig. 6. Zoom-in illustration of Fig. 5.

top 10 optimal wavelength sets were chosen based on the criteria [Eq. (14)].

Likewise, top 10 combination sets of six wavelengths also were selected from extreme points with large R and small κ. Table 4 indicates that top 10 optimal wavelength sets comprise 11 wavelengths of the diodes: 650, 705, 730, 850, 852, 860, 870, 880, 905, 915, and 937 nm. The combination of 650, 705, 730, 870, 915, and 937 nm is the first choice for the optimal wavelength set; in this case, 870 or 880 nm is only the difference for the first or second choice.

3. Seven Wavelength Sets

Here we demonstrate the scatterplot of the residual and condition number of seven wavelengths (Figs. 7 and 8) according to Eqs. (10) and (12), in which the optimal region was

Table 3. Top 10 Different Sets of Laser Diodes with Five Wavelengths

	R	κ	Wavelengths
1	0.4193	14.70	650, 705, 880, 915, 937
2	0.4188	13.99	650, 705, 870, 915, 937
3	0.4173	13.72	650, 730, 870, 915, 937
4	0.4169	26.43	650, 705, 860, 905, 937
5	0.4164	14.37	650, 730, 880, 915, 937
6	0.4164	13.83	650, 705, 860, 915, 937
7	0.4141	13.97	650, 705, 852, 915, 937
8	0.4140	14.03	650, 705, 850, 915, 937
9	0.4130	13.56	650, 730, 860, 915, 937
10	0.4079	13.68	650, 730, 852, 915, 937

Table 4. Top 10 Different Sets of Laser Diodes with Six Wavelengths

	R	κ	Wavelengths
1	0.5598	13.97	650, 705, 730, 870, 915, 937
2	0.5577	14.61	650, 705, 730, 880, 915, 937
3	0.5557	13.81	650, 705, 730, 860, 915, 937
4	0.5504	13.93	650, 705, 730, 852, 915, 937
5	0.5500	14.00	650, 705, 730, 850, 915, 937
6	0.5453	25.91	650, 705, 730, 860, 905, 937
7	0.5408	25.87	650, 705, 730, 808, 880, 915
8	0.5401	24.82	650, 705, 730, 816, 880, 915
9	0.5388	26.29	650, 705, 730, 852, 905, 937
10	0.5377	26.53	650, 705, 730, 850, 905, 937

Table 5. Top 10 Different Sets of Laser Diodes with Seven Wavelengths

	R	κ	Wavelengths
1	0.6204	14.33	650, 690, 705, 730, 870, 915, 937
2	0.6183	14.98	650, 690, 705, 730, 880, 915, 937
3	0.6166	14.18	650, 690, 705, 730, 860, 915, 937
4	0.6117	14.31	650, 690, 705, 730, 852, 915, 937
5	0.6113	14.37	650, 690, 705, 730, 850, 915, 937
6	0.6077	26.65	650, 690, 705, 730, 860, 905, 937
7	0.6065	14.37	650, 685, 705, 730, 870, 915, 937
8	0.6046	15.02	650, 685, 705, 730, 880, 915, 937
9	0.6027	14.22	650, 685, 705, 730, 860, 915, 937
10	0.6022	26.20	650, 690, 705, 730, 816, 880, 915

chosen, and top 10 optimal wavelength sets were identified based on the criteria [Eq. (14)].

As shown in Table 5, top 10 different combination sets of seven wavelengths were selected from extreme points with large R and small κ. As presented in Table 5, top 10 optimal wavelength sets are composed of 14 wavelengths of the diodes: 650, 685, 690, 705, 730, 816, 850, 852, 860, 870, 880, 905, 915, and 937 nm. The combination of seven wavelengths—650, 690, 705, 730, 870, 915, and 937 nm—is selected as the first choice for the optimal wavelength set; again, 870 or 880 nm is the only difference for the first or second choice in this case.

Moreover, the calculation has been performed under the condition of [10], and the same top 10 optimal five-, six-, or seven-wavelength sets can be obtained, as shown in Tables 3–5. In summary, we suggest that seven wavelengths of laser diodes with 650, 690, 705, 730, 870/880, 915, and 937 nm be recommended in the limited-budget research team for a spectral NIR tomographic imaging system operated in the CW domain to estimate chromophores in five, six, or seven wavelengths.

Additionally, the condition of elderly women was considered as well, and the corresponding outcomes are described in the following section.

B. Under the Condition of Elderly Women

In the following, we directly list top 10 sets of optimal five, six, and seven wavelengths in Tables 6–8, respectively, based on the procedure of Fig. 2.

As can be seen, the best choice for a five-wavelength set is the set consisting of 650, 705, 880, 915, and 937 nm, while the second choice is the set of 870 nm replacing 880 nm. As well, 650, 705, 730, 870, 915, and 937 nm are the supreme combination of six wavelengths. The laser diode of 690 nm can be added to the six-wavelength set to form the best seven-wavelength set. It is worth noting that 880 nm replacing 870 nm is the choice for the second best one.

In summary, we suggest that a limited-budget laboratory select multiple wavelength laser diodes 650, 705, 870 (or 880), 915, and 937 nm and always keep in the list five-, six- and seven-wavelength sets. For the six-wavelength set, 730 nm is included, and 690 nm is further added for the seven-wavelength set.

Table 6. Top 10 Different Sets of Laser Diodes with Five Wavelengths for the Condition of Elderly Women

	R	κ	Wavelengths
1	0.4193	25.90	650, 705, 880, 915, 937
2	0.4189	43.77	650, 705, 870, 905, 937
3	0.4188	25.52	650, 705, 870, 915, 937
4	0.4187	47.00	650, 705, 880, 905, 937
5	0.4173	25.34	650, 730, 870, 915, 937
6	0.4169	42.84	650, 705, 860, 905, 937
7	0.4164	25.69	650, 730, 880, 915, 937
8	0.4164	25.33	650, 705, 860, 915, 937
9	0.4145	43.28	650, 705, 852, 905, 937
10	0.4143	43.60	650, 705, 850, 905, 937

Table 7. Top 10 Different Sets of Laser Diodes with Six Wavelengths for the Condition of Elderly Women

	R	κ	Wavelengths
1	0.5598	25.62	650, 705, 730, 870, 915, 937
2	0.5577	25.97	650, 705, 730, 880, 915, 937
3	0.5557	25.44	650, 705, 730, 860, 915, 937
4	0.5504	25.41	650, 705, 730, 852, 915, 937
5	0.5500	25.42	650, 705, 730, 850, 915, 937
6	0.5481	42.93	650, 705, 730, 870, 905, 937
7	0.5453	42.12	650, 705, 730, 860, 905, 937
8	0.5396	45.51	650, 705, 730, 880, 905, 937
9	0.5388	42.44	650, 705, 730, 852, 905, 937
10	0.5377	42.70	650, 705, 730, 850, 905, 937

Table 8. Top 10 Different Sets of Laser Diodes with Seven Wavelengths for the Condition of Elderly Women

	R	κ	Wavelengths
1	0.6204	25.96	650, 690, 705, 730, 870, 915, 937
2	0.6183	26.30	650, 690, 705, 730, 880, 915, 937
3	0.6166	25.79	650, 690, 705, 730, 860, 915, 937
4	0.6117	25.75	650, 690, 705, 730, 852, 915, 937
5	0.6113	25.77	650, 690, 705, 730, 850, 915, 937
6	0.6102	43.64	650, 690, 705, 730, 870, 905, 937
7	0.6077	42.84	650, 690, 705, 730, 860, 905, 937
8	0.6065	25.99	650, 685, 705, 730, 870, 915, 937
9	0.6046	26.33	650, 685, 705, 730, 880, 915, 937
10	0.6027	25.82	650, 685, 705, 730, 860, 915, 937

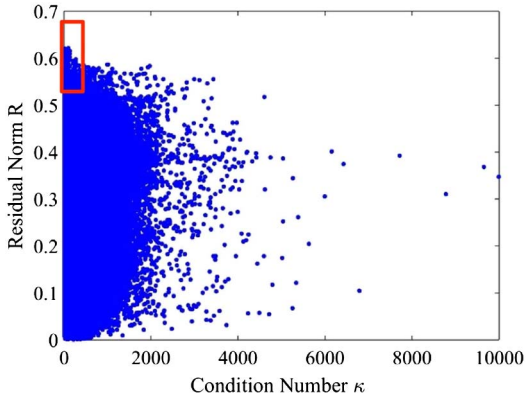

Fig. 7. Scatterplot of the residual and condition number; each point represents a different combination set of laser diodes with seven wavelengths.

C. Further Comparison and Interpretation

Compare the multiwavelength sets between young and elderly women; it is noted that, for the selection of five-, six-, and seven-wavelength diodes, the first five sets are all the same. This implies that the optimum laser-diode sets (five-, six-, and seven-wavelength) are effective for both young and elderly women.

To highlight the selected diode set, the first five wavelengths are indicated by solid lines on the chromophore absorption diagram; besides, the first six- and seven-wavelength sets are plotted with adding dot–dash and dash lines in Fig. 9. As can be seen, [HbO_2] and [HbR] are a hundred to a thousand times of [H_2O] and [Lipid]. It is observed that these lines are distributed far from the concurrent point (~800 nm) for HbO_2 and HbR, thereby expanding the absorption difference between HbO_2 and HbR to be capable of revealing their characteristics; however, they are close to the concurrent points (~670 and 930 nm) for water and lipid. As known, the optical-property images of [HbO_2] and [HbR] better enable us to characterize tissue conditions than [H_2O] and [Lipid].

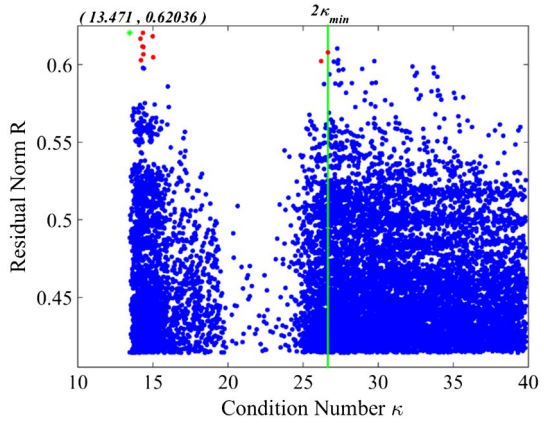

Fig. 8. Zoom-in illustration of Fig. 7.

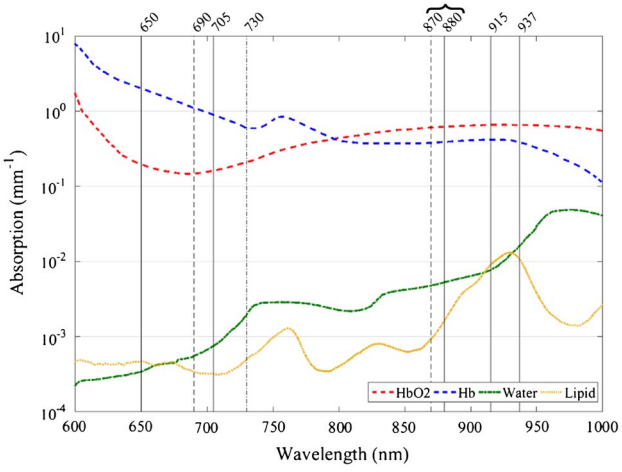

Fig. 9. Absorption spectra of main tissue constituents in the 600–1000 nm spectral range with an indication of optimal five, six, and seven wavelengths.

The histograms of appropriate wavelengths to be employed in constructing a spectral NIR tomographic imaging system are evaluated from Tables 3–5 and Tables 6–8, respectively, for young and elderly women. It is found that the wavelengths of 650, 937, and 705 nm count 30, 30, and 26 times for the young, and 30, 30, and 28 times for the elderly; thus, it implies that these three wavelengths can be considered as the top three wavelengths to select. It is worth noting that the chromophores of water and lipids possess low but similar absorption nature, whereas HbO_2 and HbR possess a high and distinct one.

Therefore, from the first choice viewpoint and the histogram counts, a general guide to select optimal wavelengths for the CW spectral NIR tomographic system can be made, i.e., choosing the wavelengths that hold distinct absorption between HbO_2 and HbR.

D. Reconstructions from Simulated Data with Optimal and Nonoptimal Sets of Wavelengths

In this section, simulated data were used to validate the above claims, the benefits brought by the derived optimal set of wavelengths on the reconstruction images. We considered two nonoptimal sets and one optimal set of five wavelengths, i.e., (Set 1) the first nonoptimal set chosen from low values of R and κ, (Set 2) the second nonoptimal set from high values of R and κ, and (Set 3) the optimal set from high value of R and low value of κ. Table 9 lists these wavelength sets.

In the following two reconstruction tests, an 80 mm diameter phantom with background chromophore concentrations of young and elderly women, respectively, as listed in Table 2, was employed. Further, the use of background scattering parameters follows Eq. (7) with scattering amplitude $A = 1$ mm^{-1} and scattering power $s_p = 1.3$. Figure 10 shows five 15 mm diameter circular inclusions embedded in the designated phantom for the case of background with various chromophore concentrations of young women. In the four of five inclusions, each of

Table 9. Nonoptimal (Sets 1 and 2) and Optimal (Set 3) Sets of Five-Wavelength Laser Diodes Chosen for Reconstruction

Wavelength Set	Wavelengths
1	780, 850, 852, 915, 937
2	650, 685, 690, 785, 850
3	650, 705, 880, 915, 937

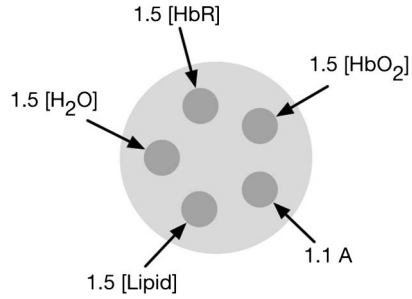

Fig. 10. Designated 2D circular phantom used in the simulation test (case of young women).

the chromophore concentrations (HbO_2, HbR, water, and lipids) possesses 50% higher concentration with respect to its background; for the fifth one, its scattering amplitude is 10% higher.

Images of chromophore concentrations and scattering parameters were reconstructed by the modified in-house-coded reconstruction program [15], which implements the computation schemes described in the previous section. Finite-element forward solution using the mesh consisting of 4225 nodes and 8192 triangle elements generated simulated CW data at 16 source and detector positions equally spaced along the circumference of phantom. To imitate the more practical situation, 3% random Gaussian noise was added to the synthesized data. A second mesh with 817 nodes and 1536 triangle elements was generated and employed in the inverse problem for image reconstruction. All the reconstructed images reported here were reconstructed initially from homogeneous optical properties. For all cases, 20 iterations were used during the inverse

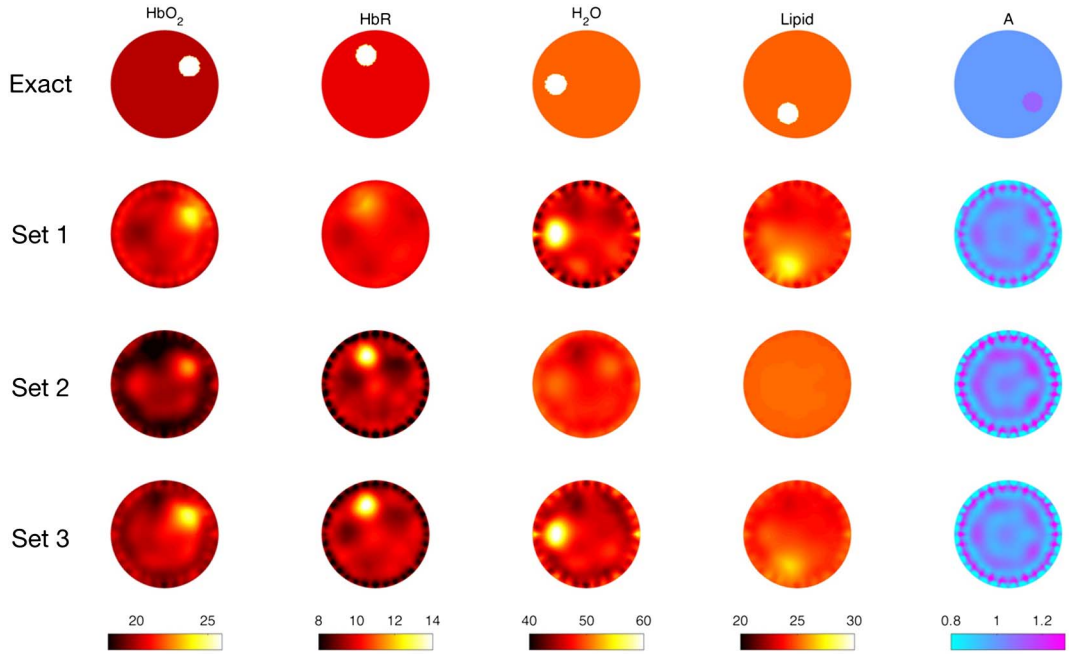

Fig. 11. Image reconstruction of 2D circular phantom with various background chromophore concentrations for young women.

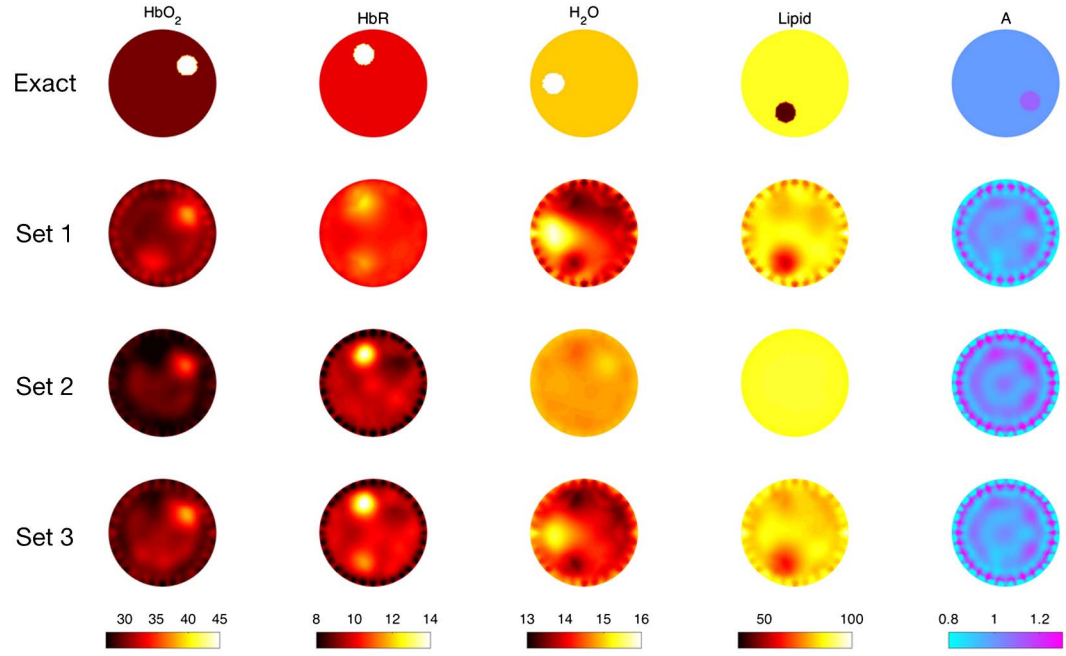

Fig. 12. Image reconstruction of 2D circular phantom with various background chromophore concentrations for elderly women.

computation. Note that, in the work presented here, the scattering power s_p kept as a constant throughout the problem. For this reason, the scattering power s_p was set as a constant value in the reconstruction, i.e., the scattering amplitude A is the only scattering parameter to be reconstructed during iterations.

Figure 11 shows the reconstructed images for the background chromophore concentrations of young women. The top row illustrates the designated inclusion locations in the phantom, and the lower rows show the reconstruction results with using different wavelength sets. A low reconstructed contrast for the HbR inclusion is present when wavelength Set 1 is employed. The inclusions with the higher contrast of water or lipids cannot not be effectively reconstructed by using wavelength Set 2. As expected, the reconstruction through the proposed optimal wavelength Set 3 yields the best contrast for distinguishing various chromophores.

Reconstructed images for the background chromophore concentrations of elderly women are shown in Fig. 12. Note that, in this case, due to the high percentage of background lipids for elderly women, lipid contrast in the inclusion is reduced 50% rather than increased. It is found that, when wavelength Set 1 is used, low reconstructed contrast for the HbR inclusion is characterized; moreover, a cross-talk phenomenon is presented in the HbO_2 and HbR images. Likewise, the inclusion with water or lipid contrast also fails in the reconstruction through using wavelength Set 2. Again, the best contrast for various chromophores can be obtained when the proposed optimal wavelength Set 3 is employed for reconstruction.

4. CONCLUSION

In this paper, we have studied the selection of optimum wavelength diode sets, a procedure to choose the best measurement wavelengths for reconstructing the images of chromophores, HbO_2 and HbR, H_2O, and lipids. Compared with the available but high-priced broadband laser systems, it is nontrivial to select the most appropriate wavelength sets from existing commercial cost-effective laser diodes. Here, a total of 38 wavelengths have been considered to designate five-, six-, and seven-wavelength optimized sets. More included wavelengths have proved to be a reliable way to compensate for under- or over-estimation of the chromophore concentrations in the spectral image reconstruction. Furthermore, an optimized set with five wavelengths is more computation efficient than the set with seven wavelengths. Consequently, the five-wavelength optimized set is preferable, especially for limited-budget research groups. Simulated data for young and elderly women cases with using two nonoptimal sets and one optimal set of five wavelengths were applied to validate our claims. In conclusion, to build up a cost-effective spectral NIR tomographic system in the CW domain choosing the laser diodes with the wavelengths of 650, 690, 705, 730, 870/880, 915, and 937 nm for both young and elderly women is recommended.

Funding. Ministry of Science and Technology (MOST) (NSC101-2221-E-008-093-MY3, MOST103-2221-E-236-010).

REFERENCES

1. Y. Yamashita, A. Maki, and H. Koizumi, "Wavelength dependence of the precision of noninvasive optical measurement of oxy-, deoxy-, and total-hemoglobin concentration," Med. Phys. **28**, 1108–1114 (2001).
2. H. Sato, M. Kiguchi, F. Kawaguchi, and A. Maki, "Practicality of wavelength selection to improve signal-to-noise ratio in near-infrared spectroscopy," NeuroImage **21**, 1554–1562 (2004).
3. A. Pifferi, P. Taroni, A. Torricelli, F. Messina, R. Cubeddu, and G. Danesini, "Four-wavelength time-resolved optical mammography in the 680-980-nm range," Opt. Lett. **28**, 1138–1140 (2003).
4. K. Uludağ, J. Steinbrink, A. Villringer, and H. Obrig, "Separability and cross talk: optimizing dual wavelength combinations for near-infrared spectroscopy of the adult head," NeuroImage **22**, 583–589 (2004).
5. P. Taroni, G. Danesini, A. Torricelli, A. Pifferi, L. Spinelli, and R. Cubeddu, "Clinical trial of time-resolved scanning optical mammography at 4 wavelengths between 683 and 975 nm," J. Biomed. Opt. **9**, 464–473 (2004).
6. A. Corlu, R. Choe, T. Durduran, K. Lee, M. Schweiger, S. R. Arridge, E. M. Hillman, and A. G. Yodh, "Diffuse optical tomography with spectral constraints and wavelength optimization," Appl. Opt. **44**, 2082–2093 (2005).
7. A. Corlu, T. Durduran, R. Choe, M. Schweiger, E. M. Hillman, S. R. Arridge, and A. G. Yodh, "Uniqueness and wavelength optimization in continuous-wave multispectral diffuse optical tomography," Opt. Lett. **28**, 2339–2341 (2003).
8. M. E. Eames, J. Wang, B. W. Pogue, and H. Dehghani, "Wavelength band optimization in spectral near-infrared optical tomography improves accuracy while reducing data acquisition and computational burden," J. Biomed. Opt. **13**, 054037 (2008).
9. B. Brendel and T. Nielsen, "Selection of optimal wavelengths for spectral reconstruction in diffuse optical tomography," J. Biomed. Opt. **14**, 034041 (2009).
10. A. Li, G. Boverman, Y. Zhang, D. Brooks, E. L. Miller, M. E. Kilmer, Q. Zhang, E. M. Hillman, and D. A. Boas, "Optimal linear inverse solution with multiple priors in diffuse optical tomography," Appl. Opt. **44**, 1948–1956 (2005).
11. K. D. Paulsen and H. Jiang, "Spatially varying optical property reconstruction using a finite element diffusion equation approximation," Med. Phys. **22**, 691–701 (1995).
12. Extinction Coefficients, http://omlc.ogi.edu/spectra
13. B. J. Tromberg, N. Shah, R. Lanning, A. Cerussi, J. Espinoza, T. Pham, L. Svasaand, and J. Butler, "Non-invasive in vivo characterization of breast tumors using photon migration spectroscopy," Neoplasia **2**, 26–40 (2000).
14. P. Taroni, A. Pifferi, A. Torricelli, D. Comelli, and R. Cubeddu, "In vivo absorption and scattering spectroscopy of biological tissues," Photochem. Photobiol. Sci. **2**, 124–129 (2003).
15. L. Y. Chen, M.-C. Pan, and M.-C. Pan, "Flexible near-infrared diffuse optical tomography with varied weighting functions of edge-preserving regularization," Appl. Opt. **52**, 1173–1182 (2013).